Int. J. Electron. Commun. (AEÜ) 75 (2017) 35–45

Contents lists available at ScienceDirect

International Journal of Electronics and Communications (AEÜ)

journal homepage: www.elsevier.com/locate/aeue

Regular paper

Precision of direction of arrival (DOA) estimation using novel three dimensional array geometries

Sarah Poormohammad, Forouhar Farzaneh *

Department of Electrical Engineering, Sharif University of Technology, Tehran 11155-4363, Iran

ARTICLE INFO

Article history:
Received 23 October 2016
Accepted 28 February 2017

Keywords:
Radio direction finding
DOA
Three dimensional (3D) arrays
Array geometry
Subspace-based DOA
MUSIC
Monte-Carlo simulation
Smart antennas

ABSTRACT

Numerous methods for direction of arrival (DOA) estimation, used in smart antennas have been already reported in previous studies. The precision of DOA estimation depends on the choice of the algorithm and the geometrical configuration of the antenna array. In this work, the performance of new geometrical configurations, i.e. 2D with equal area and 3D with equal volume including circular, square, triangular, hexagonal and star geometries, with equal number of antenna elements, are examined and compared to each other to find the most proper geometry. Monte-Carlo simulations are performed to evaluate the DOA precision of the proposed arrays using the MUSIC algorithm. It is shown that in three cases of comparison including 2D geometries, 3D geometries and 3D rotated geometries, with the star and triangular configurations one achieves better resolution in DOA estimation. It is also revealed that the rotated configurations show lower estimation error compared to normal configurations.

1. Introduction

Smart antennas have several advantages in wireless applications such as higher system capacity, higher signal to interference ration (SIR), lower power signals and greater data rate. Smart antennas can be used to enhance the accuracy of direction of arrival estimation in presence of different interferences. The angular resolution of different sources can be used to combine signals for better fidelity, suppress interferences or both to enhance the capacities of systems [1].The precision and the stability of DOA estimation have an important role in smart antenna applications. In the past years different solutions were established to find an optimal DOA algorithm. Some early solutions based on spectral estimation such as Bartlett, Maximum-likelihood and linear prediction methods were reported in [2]. Another high resolution method which is based on maximizing signal-to-interference ratio is known as Capon or MVDR method [3]. Other accurate and efficient methods and their variants like MUSIC [4] and ESPRIT [5], [6] have been studied widely over the past decades. The performance evaluation of MUSIC and ESPRIT estimation methods was reported in [7]. The two methods have greater resolution and greater accuracy than the other classical methods like Bartlett and CAPON. The simulations in [8] indicate that the MUSIC algorithm is more accurate and stable compared to the ESPRIT algorithm for uniform linear array case. In general the quality of DOA estimation is affected by the choice of the algorithm, number of antenna elements, number of sources, the SNR, number of snapshots and the geometry of array configuration. Regarding the geometry most of the studies for DOA estimations have been established for uniform linear arrays (ULAs) and uniform rectangular arrays (URAs). ULAs configuration has the limitation of DOA estimating only in one direction. For 2D estimation, planar arrays like uniform rectangular arrays and uniform circular arrays have been proposed in [9],[10]. The comparison in [9] revealed that the planar UCA achieved the deepest nulls toward the angles of interference and had a better performance than the rectangular array. The impact of geometries on DOA estimation was studied first by Manikas [11]. In [11] authors considered six types of geometry including linear, circular, Y-shaped and X-shaped, dual ring and dual spiral arrays, and compared these geometries in terms of Cramer-Rao Bound and the resolution and the detection threshold as a function of azimuth angle of arrival. In [12] the authors performed simulations to show that the Two L-Shaped Array (TLSA) has a better Cramer-Rao Lower-Bound (CRLB) for two-dimensional (2-D) direction-of-arrival (DOA) estimation than other array configurations. In particular, MUSIC algorithm was established to compare the capabilities of circular and uniform Y-shaped and non-uniform Y-shaped array including the mutual coupling in [13] and it was concluded that the circular array has the

* Corresponding author.
E-mail address: farzaneh@sharif.edu (F. Farzaneh).

http://dx.doi.org/10.1016/j.aeue.2017.02.013
1434-8411/

best performance. In [14] a novel configuration known as semi-circular array was compared to circular array with Capon DOA estimation algorithm and simulation results showed that the proposed array achieved 50% better resolution than the circular array. In [15] a comparative study of different planar antenna arrays and three dimensional 2L-shaped array has been presented. The study shows that the proposed three dimensional geometry known as 2L-shaped array can be about 5 dB better in SNR than the L-shaped two dimensional array used in [16]. In [17] a Modified Root-MUSIC algorithm is proposed to estimate the angle of arrival and the polarization of the plane waves with diversely polarized uniform circular array (UCA) in the presence of mutual coupling effects between antenna arrays. In [18] authors present a 2-D angle of arrival estimation method for the L-shaped array based on tensor decomposition, benefiting from multiple invariance feature of array manifold which leads to a better performance than the other 2-D angle of arrival estimation algorithms. In addition MUSIC algorithm based on spatial time-frequency distribution (STFD) has been investigated for direction of arrival (DOA) estimation of closely-spaced sources. A short-time Fourier transform (STFT) based MUSIC algorithm was proposed in [19] with a low implementation complexity and small number of sensors.

In this study our objective is to develop new two or three dimensional geometries for the design of antenna arrays that could

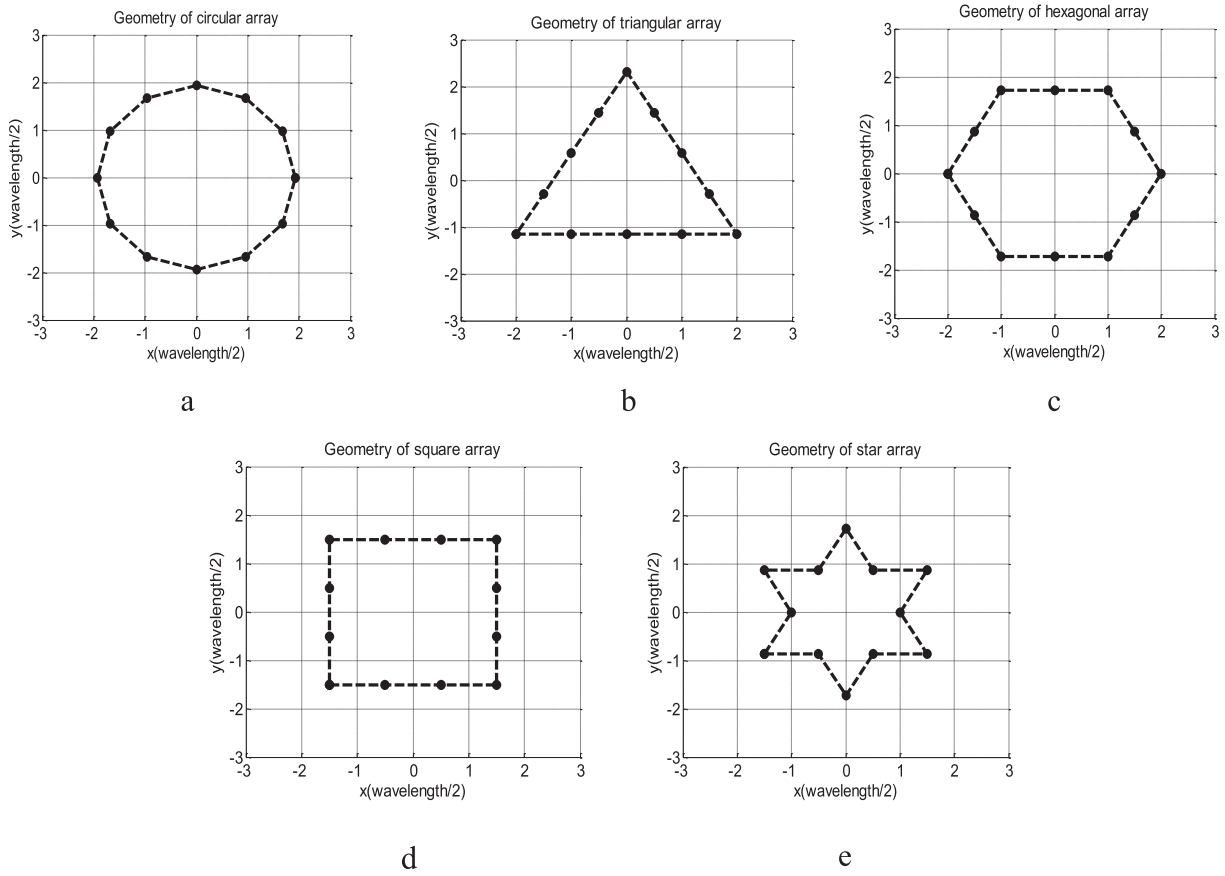

Fig. 1. Planar array configurations surveyed in this study, circular, triangular, hexagonal, square and star geometries. a) Circular array. b) Triangular array. c) Hexagonal array. d) Square array. e) Star array.

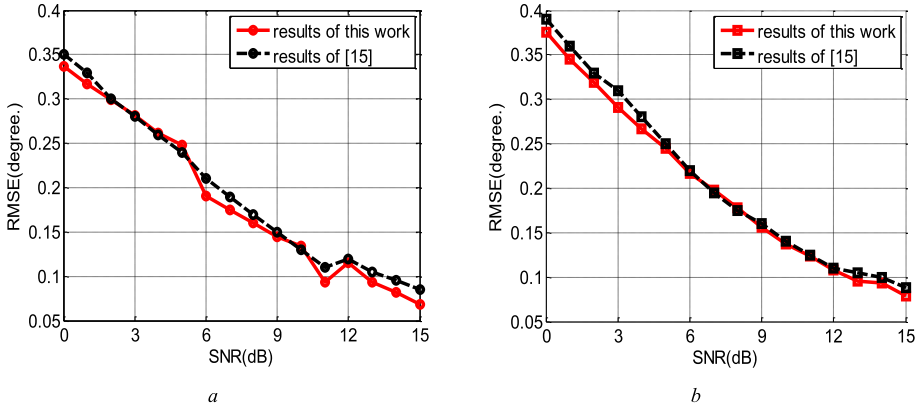

Fig. 2. Comparison of the simulation results of this work with those of [15] as a function of SNR for (a) circular array, (b) rectangular array with 8 elements.

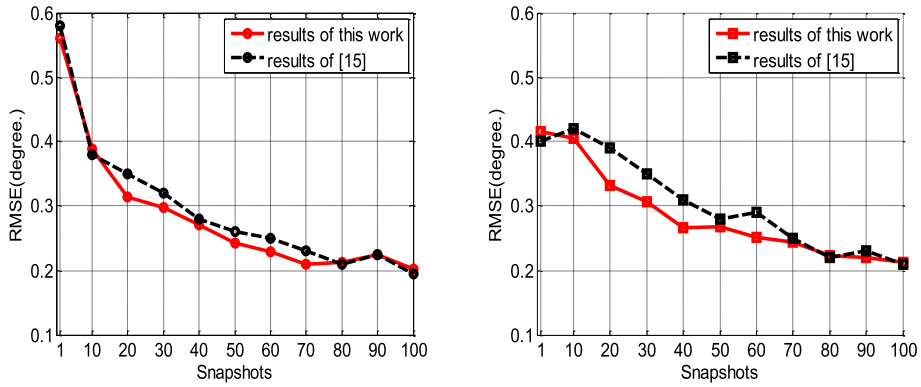

Fig. 3. Comparison of the simulation results of this work with those of [15] as a function of snapshots for (a) circular array, (b) rectangular array with 8 elements.

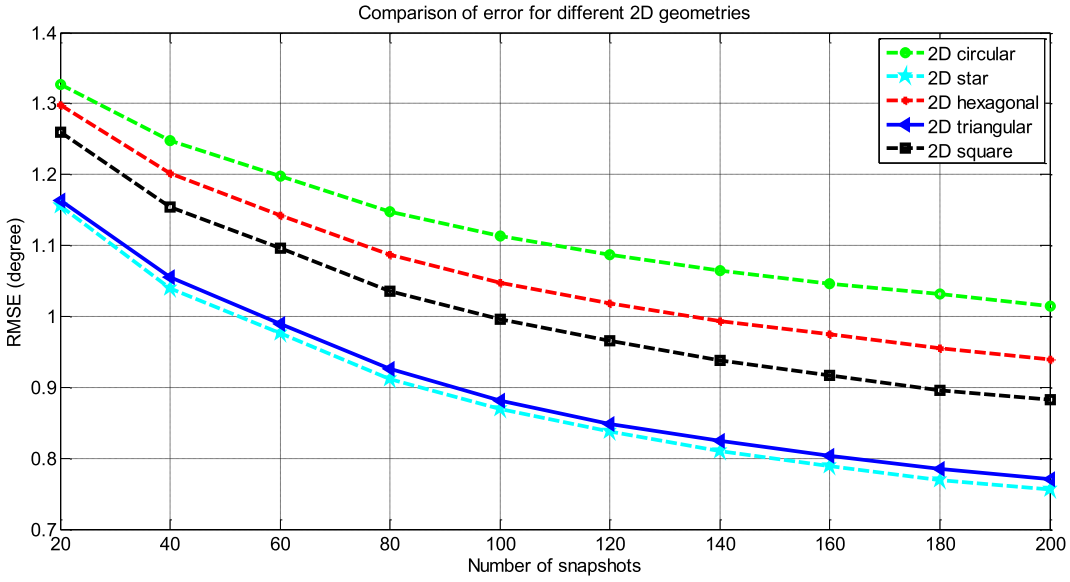

Fig. 4. RMSE versus the number of snapshots for 2D geometries with fixed SNR = 7 dB.

improve the accuracy of DOA estimation for both azimuth and elevation angles. The goal of the design is to achieve a high resolution estimation with well established consistency. We have studied different array geometries including the circular, the triangular, the square, the hexagonal and the star ones and we have compared their corresponding performances in the related scenarios for both azimuth and elevation estimation. In the next step, three dimensional design of the proposed arrays and their rotated forms are presented and compared to the conventional three dimensional configurations of circular, square and triangular cylindrical geometries. This study shows that among the planar designs, the star geometry configuration has a better performance compared to the other four planar arrays. Obviously, three dimensional arrays show better resolution than their two dimensional counterparts in each case. Another novel design presented here is the three dimensional antenna array with rotated cross sectional configuration. Monte-Carlo simulations show that the rotation of antenna's cross sections (slices) about the z-axis has a great impact on the accuracy of DOA estimation.

The paper is followed within the next three sections. Section 2 presents the signal model and the direction finding algorithm of the proposed arrays. Section 3 presents the array geometries and the corresponding numerical simulations to compare the performances of the proposed arrays and the demonstration of superiority of the novel geometries. Finally, Section 4 draws the conclusion.

Table 1
The average of estimation error for Fig. 4.

Geometry	Average of estimation error (°)
Circular	1.123
Hexagonal	1.060
Square	1.008
Triangular	0.898
Star	0.884

2. Signal model and direction finding algorithm

2.1. Signal model

Consider there are D uncorrelated, narrow band signal sources arriving from D directions at angles θ_i and φ_i and received by an array of M elements with their potential weights. Each signal received by the array is known as $x_m(k)$ including additive, zero mean, Gaussian noise and the variation in time domain is represented by k'th time sample. In matrix form, the output of the array can be given in the following form:

$$\boldsymbol{y_k} = \bar{\boldsymbol{w}}^T \cdot \bar{\boldsymbol{x}} \tag{1}$$

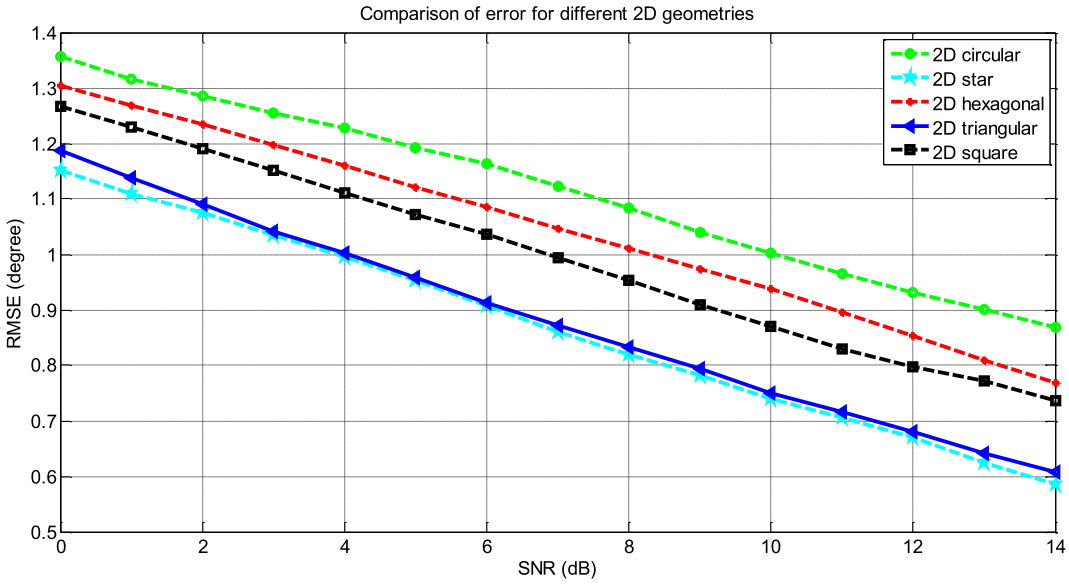

Fig. 5. RMSE versus SNR for 2D geometries with L = 100 snapshots.

where

$$\bar{\boldsymbol{x}}(k)=[\bar{\boldsymbol{a}}(\theta_1,\varphi_1)\bar{\boldsymbol{a}}(\theta_2,\varphi_2)\cdots\bar{\boldsymbol{a}}(\theta_D,\varphi_D)]\cdot\begin{bmatrix}\boldsymbol{ls}_1(k)\\ \boldsymbol{s}_2(k)\\ \vdots\\ \boldsymbol{s}_D(k)\end{bmatrix}+\bar{\boldsymbol{n}}(k)=\bar{\boldsymbol{A}}\cdot\bar{\boldsymbol{s}}(k)+\bar{\boldsymbol{n}}(k) \tag{2}$$

and the array weights are:

$$\bar{\boldsymbol{w}}=[w_1w_2\cdots w_M]^T \tag{3}$$

In the above notation, $\bar{\boldsymbol{s}}(k)$ is the vector of incident complex monochromatic signals at time k and $\bar{\boldsymbol{A}}$ is the matrix of streering vectors $\bar{\boldsymbol{a}}(\theta_i,\varphi_i)$ and $\boldsymbol{n}(k)$ is considered as the noise vector at each array element m with σ_n^2 variance. By this definition **A** is a $M\times D$ matrix of steering vectors with $D<M$ values. Array elements are identical isotropic antennas. In general the steering vector $\bar{\boldsymbol{a}}(\theta_i,\varphi_i)$ with wavenumber of k_c is defined according to [1]:

$$\bar{\boldsymbol{a}}(\theta_i,\varphi_i)=e^{-jk_cr_{im}} \tag{4}$$

where

$$r_{im}=\hat{\boldsymbol{r}}_i\boldsymbol{r}_m \tag{5}$$

In this notation $\boldsymbol{r_m}$ is the position vector of each array element m and $\hat{\boldsymbol{r}}_i$ is the unit vector in the direction of the field point and they are defined as follows:

$$\boldsymbol{r}_m=x_m\hat{\boldsymbol{x}}+y_m\hat{\boldsymbol{y}}+z_m\hat{\boldsymbol{z}} \tag{6}$$

$$\hat{\boldsymbol{r}}_i=\sin\theta_i\cos\varphi_i\hat{\boldsymbol{x}}+\sin\theta_i\sin\varphi_i\hat{\boldsymbol{y}}+\cos\theta_i\hat{\boldsymbol{z}} \tag{7}$$

After this step we need to choose an appropriate algorithm for direction finding. The purpose of DOA estimation in this paper is based on defining the function that gives an indication of arrival angle [1]. This function is called the pseudospectrum, $P(\theta,\varphi)$ and we use the standard MUSIC algorithm as a high resolution eigen-structure method for direction finding purpose.

2.2. MUSIC DOA estimation

Considering a uniformly weighted array, uncorrelated noise with equal variances σ_n^2, in order to simplify the notation of (2) the array auto-correlation matrix R_{xx} was defined as follows [1]:

$$\begin{aligned}\bar{\boldsymbol{R}}_{\boldsymbol{xx}}&=\mathrm{E}[\bar{\boldsymbol{x}}.\bar{\boldsymbol{x}}^{\boldsymbol{H}}]=E[(\bar{\boldsymbol{A}}\bar{\boldsymbol{s}}+\bar{\boldsymbol{n}})(\bar{\boldsymbol{s}}^{\boldsymbol{H}}\bar{\boldsymbol{A}}^{\boldsymbol{H}}+\bar{\boldsymbol{n}}^{\boldsymbol{H}})]\\&=\bar{\boldsymbol{A}}E[\bar{\boldsymbol{s}}.\bar{\boldsymbol{s}}^{\boldsymbol{H}}]\bar{\boldsymbol{A}}^{\boldsymbol{H}}+E[\bar{\boldsymbol{n}}.\bar{\boldsymbol{n}}^{\boldsymbol{H}}]\\&=\bar{\boldsymbol{A}}\bar{\boldsymbol{R}}_{\boldsymbol{ss}}\bar{\boldsymbol{A}}^{\boldsymbol{H}}+\bar{\boldsymbol{R}}_{\boldsymbol{nn}}\end{aligned} \tag{8}$$

where E [·] operator stands for the expected value, $[\cdot]^H$ operator stands for Hermitian matrix and the signal and the noise auto-correlation matrixes becomes:

$$\bar{\boldsymbol{R}}_{\boldsymbol{ss}}=E[\bar{\boldsymbol{s}}.\bar{\boldsymbol{s}}^{\boldsymbol{H}}],\quad \bar{\boldsymbol{R}}_{\boldsymbol{nn}}=E[\bar{\boldsymbol{n}}.\bar{\boldsymbol{n}}^{\boldsymbol{H}}]=\sigma_n^2\bar{\boldsymbol{I}} \tag{9}$$

If the process is ergodic, we can use time-averaged correlation instead of correlation and the correlation matrix is defined by [1]:

$$\bar{\boldsymbol{R}}_{xx}\approx\frac{1}{K}\sum_{k=1}^{K}\bar{\boldsymbol{x}}(k)\bar{\boldsymbol{x}}^{\boldsymbol{H}} \tag{10}$$

$$\bar{\boldsymbol{R}}_{ss}\approx\frac{1}{K}\sum_{k=1}^{K}\bar{\boldsymbol{s}}(k)\bar{\boldsymbol{s}}^{\boldsymbol{H}} \tag{11}$$

$$\bar{\boldsymbol{R}}_{nn}\approx\frac{1}{K}\sum_{k=1}^{K}\bar{\boldsymbol{n}}(k)\bar{\boldsymbol{n}}^{\boldsymbol{H}} \tag{12}$$

As signals were considered uncorrelated, R_{ss} is a diagonal matrix and with the above assumptions R_{xx}, is an Hermitian matrix with M eigenvalues $\lambda_1,\lambda_2,\cdots,\lambda_M$ associated with M eigenvectors $\bar{E}=[e_1e_2\cdots e_M]$. If the eigenvalues are sorted from smallest to lar-

Table 2
The average of estimation error for Fig. 5.

Geometry	Average of estimation error (°)
Circular	1.114
Hexagonal	1.045
Square	0.994
Triangular	0.881
Star	0.868

gest $\bar{E}$ is divided into two subspaces according to $\bar{E} = [\bar{E}_N \bar{E}_s]$. The first subspace $\bar{E}_N$ is composed of eigenvectors associated with the noise and is called the noise subspace. For this case with uncorrelated noise the eigenvalues are given as $\lambda_1, \lambda_2, \cdots, \lambda_M = \sigma_n^2$. The $M \times (M - D)$ dimensional subspace spanned by the noise eigenvectors is constructed as in (13).

$$\bar{\boldsymbol{E}}_N = [\bar{\boldsymbol{e}}_1 \bar{\boldsymbol{e}}_2 \cdots \bar{\boldsymbol{e}}_{M-D}] \tag{13}$$

The MUSIC algorithm's pseudospectrum as a function of the steering vector and the noise subspace matrix can be expressed as [1]:

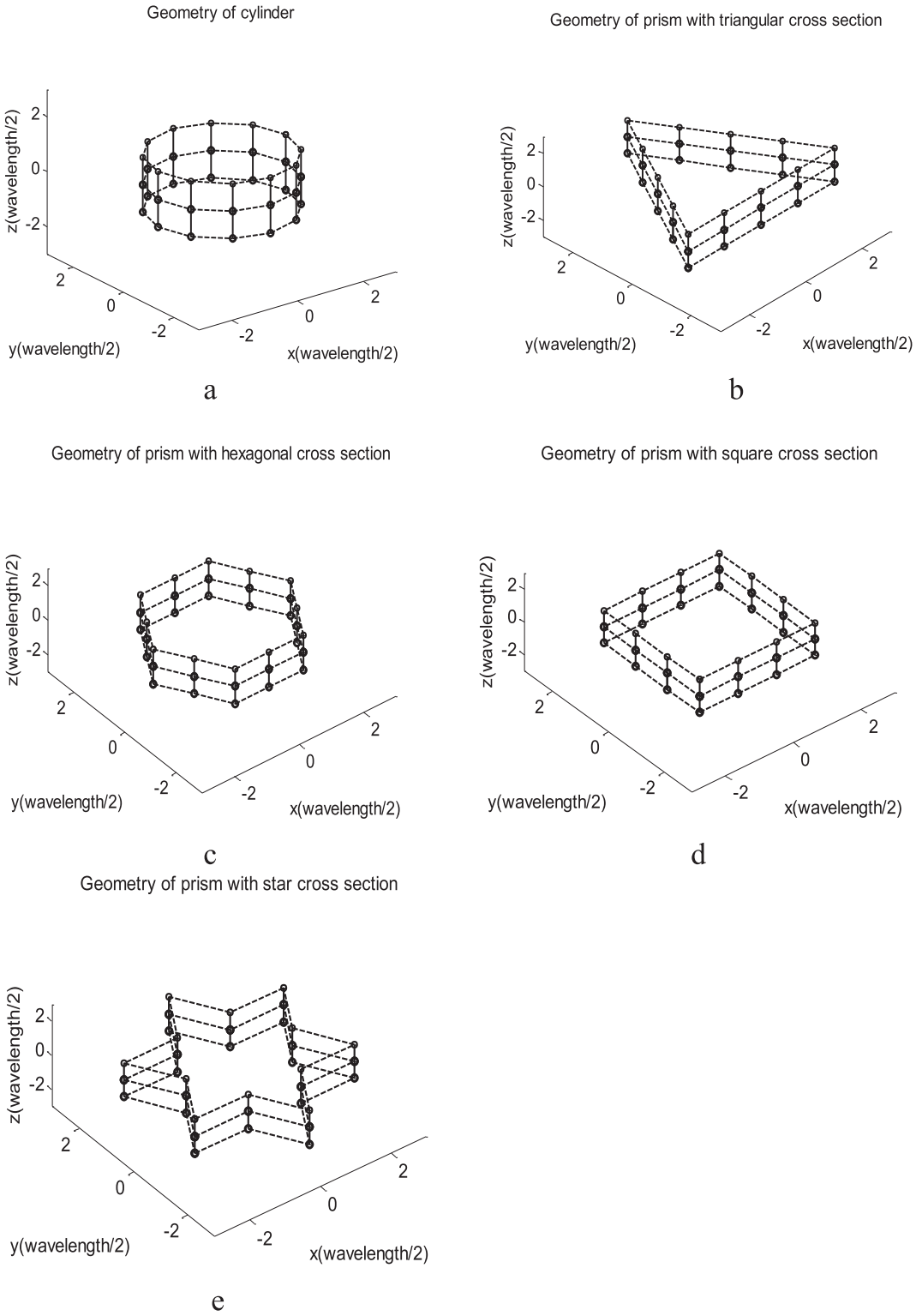

Fig. 6. Three dimensional configurations of arrays surveyed in this study, circular, triangular, square, hexagonal and star cross sections. a) 3D circular array. b) 3D triangular array. c) 3D hexagonal array. d) 3D square array. e) 3D star array

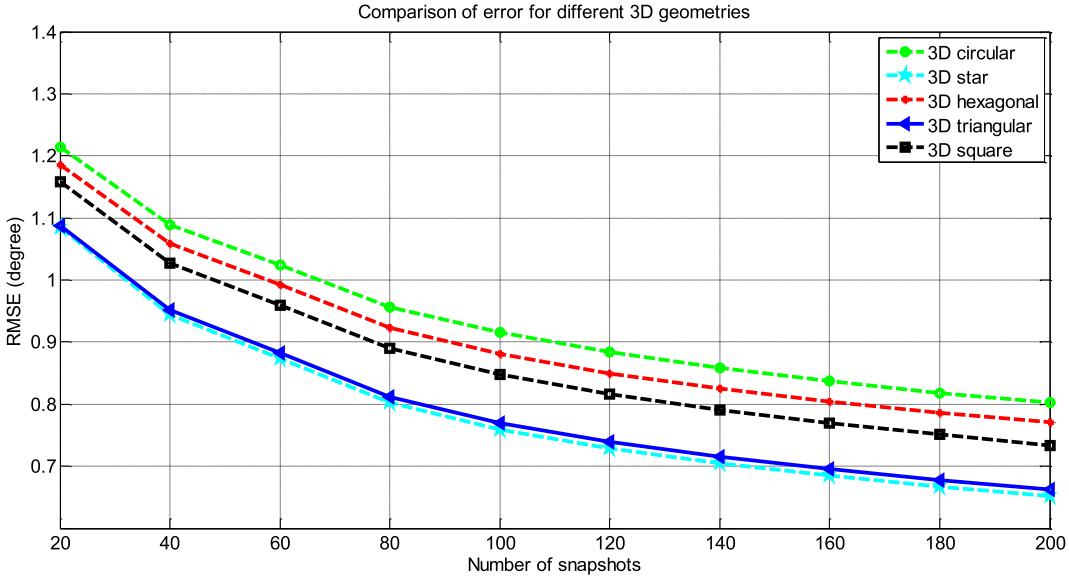

Fig. 7. RMSE versus number of snapshots for 3D geometries with SNR = 7 dB.

Table 3
The average of estimation error for Fig. 7.

Geometry	Average of estimation error (°)
Circular	1.032
Hexagonal	0.900
Square	0.867
Triangular	0.791
Star	0.781

$$\boldsymbol{P}_{MUSIC} = \frac{1}{\bar{\boldsymbol{a}}(\theta,\varphi)^{\boldsymbol{H}}\bar{\boldsymbol{E}}_N\bar{\boldsymbol{E}}_N^{\boldsymbol{H}}\bar{\boldsymbol{a}}(\theta,\varphi)} \tag{14}$$

This function has sharp maxima at the angles of arrival(for every θ,φ) of the incident signals. After finding the maxima of P_{MUSIC} as a function of θ,φ we use the root mean square error (RMSE) for a number of random arrival angles to compare the performances of different geometries.

3. Array geometries and numerical simulations

3.1. Planar arrays

In this paper we use arrays with 12 elements per array to evaluate the elevation angle and the azimuth angle of arrivals for 5 signal sources and compare the efficiency of MUSIC algorithm for DOA determination in different geometries. For two dimensional (2D) or planar arrays we assume 5 configurations as depicted in Fig. 1. The configurations of proposed arrays include circular, triangular, hexagonal, square and star geometries. We consider that the elements in the circular planar array are spaced by $\lambda/2$ and therefore the radius of the circle would be:

$$r_a = \frac{\lambda/4}{\sin\left(\frac{\pi}{12}\right)} \tag{15}$$

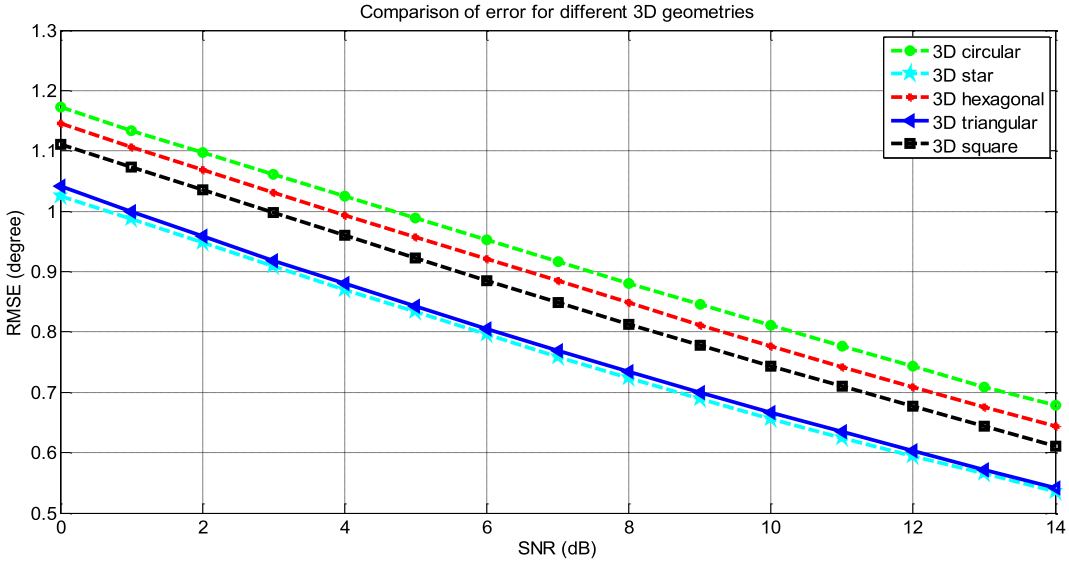

Fig. 8. RMSE versus SNR for 3D geometries with L = 100 snapshots.

Table 4
The average of estimation error for Fig. 8.

Geometry	Average of estimation error (°)
3D Circular	0.919
3D Hexagonal	0.887
3D Square	0.853
3D Triangular	0.777
3D Star	0.767

In the four remaining configurations the spacing between the elements is taken such that all the configurations would have the same areas. All the geometries are centered about the origin in the xy plane.

The position vector of antenna elements for different geometries is calculated in the Cartesian coordinates and set as x_m and y_m in equation:

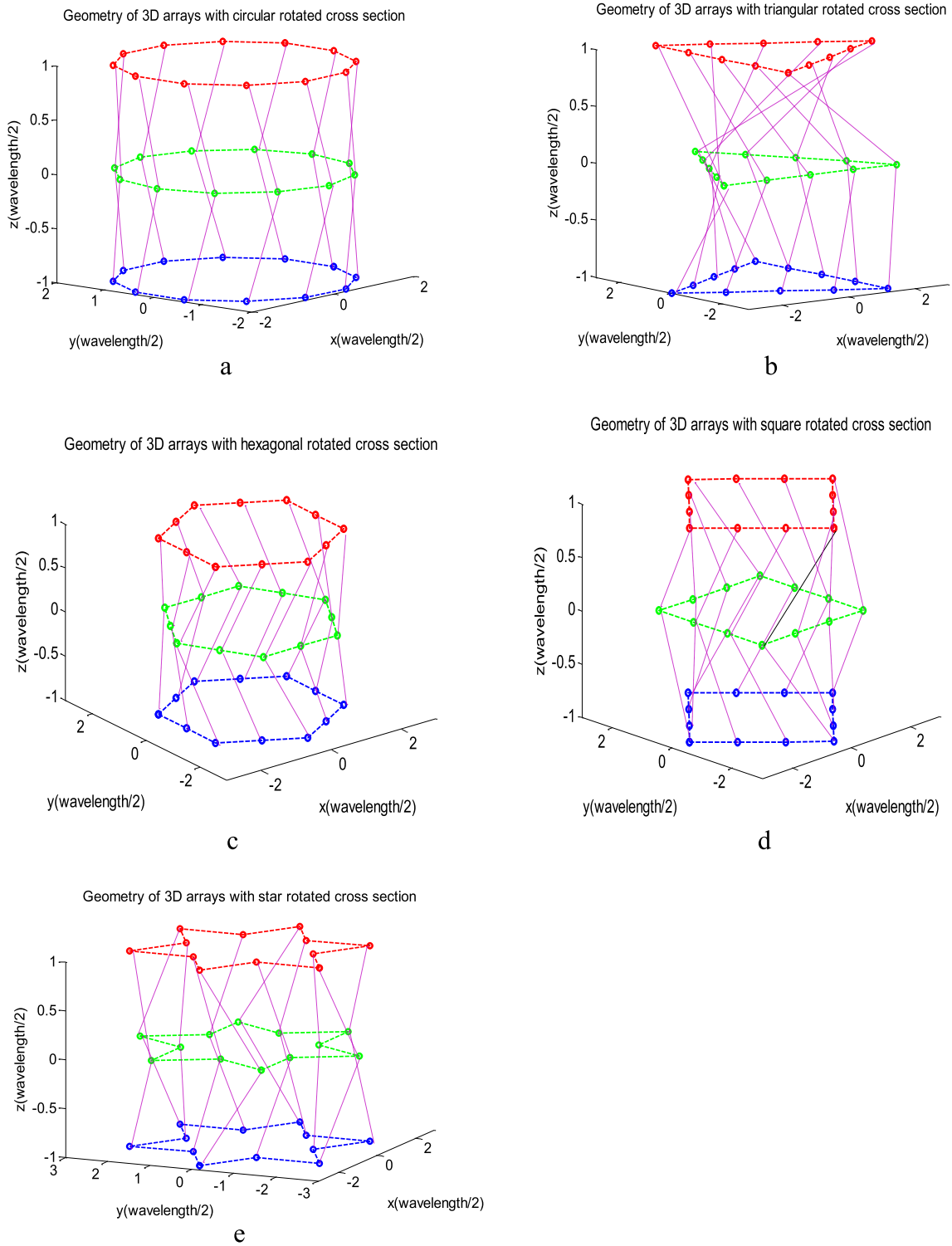

Fig. 9. Novel three dimensional configurations of rotated arrays surveyed in this study, circular, triangular, square, hexagonal and star. a) 3D rotated circular array. b) 3D rotated triangular array. c) 3D rotated hexagonal array. d) 3D rotated square array. e) 3D rotated star array.

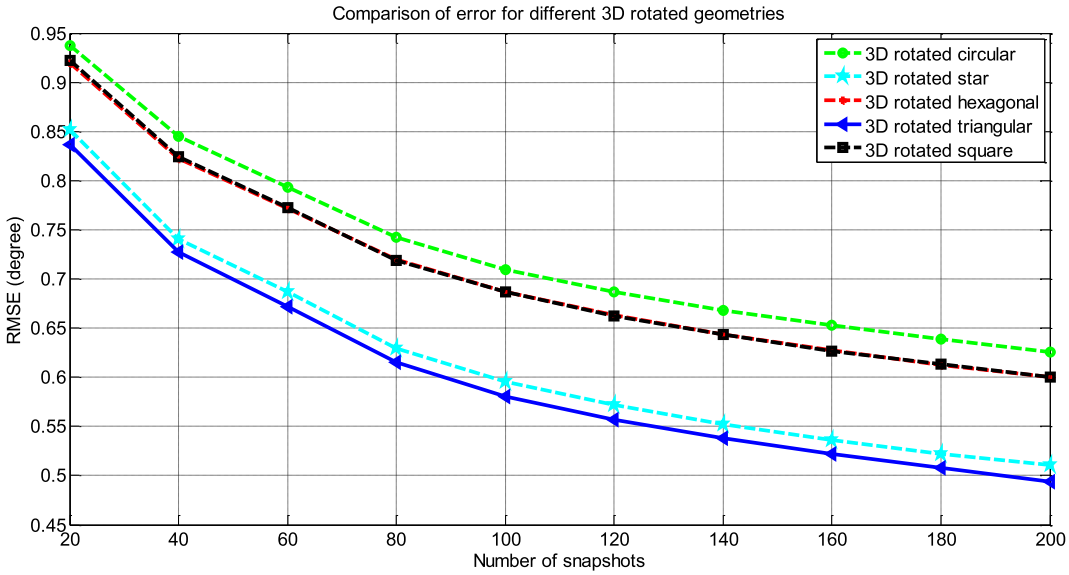

Fig. 10. RMSE versus number of snapshots for 3D rotated geometries with SNR = 7 dB.

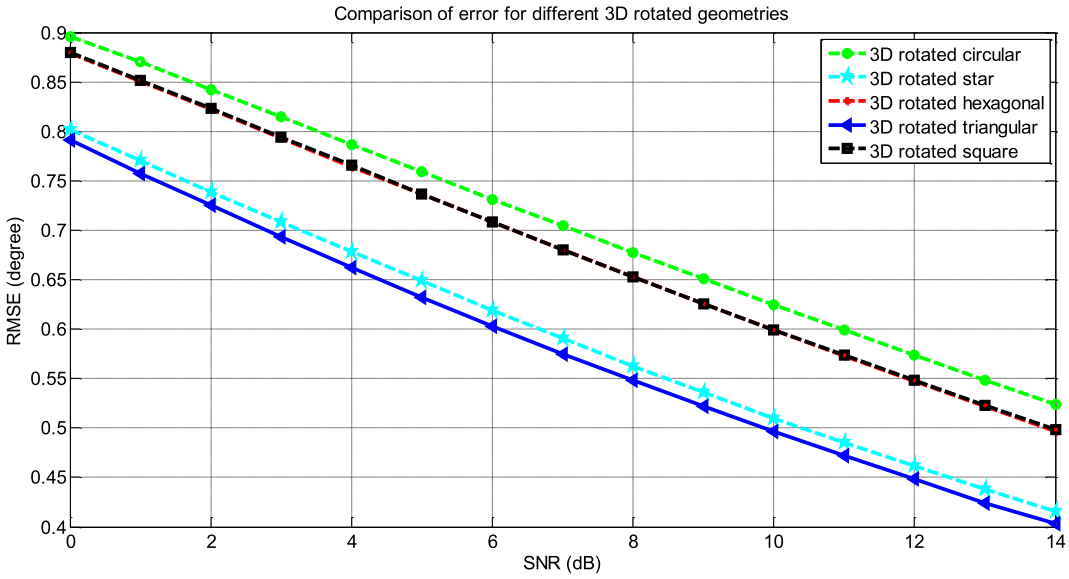

Fig. 11. RMSE versus SNR for 3D rotated geometries with L = 100 snapshots.

Table 5
The average of estimation error for Fig. 10.

Geometry	Average of estimation error (°)
3D Rotated Circular	0.724
3D Rotated Hexagonal	0.701
3D Rotated Square	0.702
3D Rotated Triangular	0.598
3D Rotated Star	0.613

Table 6
The average of estimation error for Fig. 11.

Geometry	Average of estimation error (°)
3D Rotated Circular	0.707
3D Rotated Hexagonal	0.683
3D Rotated Square	0.684
3D Rotated Triangular	0.583
3D Rotated Star	0.597

$$\boldsymbol{r}_m = x_m\hat{\boldsymbol{x}} + y_m\hat{\boldsymbol{y}} \tag{16}$$

We use root mean square error (RMSE) of joint azimuth and elevation angles to evaluate the performance of different antenna geometries in two dimensional direction finding. Resolution estimation for azimuth and elevation angle of arrivals has an important role in distinguishing between different signal directions and for this purpose we use RMSE of detected angles to compare different geometries. To verify the resolution of our algorithm for each incident signal we generate a large number of random directions, K and we compute the RMSE in each geometry as given by (17).

$$\sigma_n = \sqrt{\frac{1}{2K}\sum_{i=1}^{K}((\theta_i - \hat{\theta}_i)^2 + ((\varphi_i - \hat{\varphi}_i)^2)} \tag{17}$$

For the N simultaneous incident signals the RMSE is averaged again by (18).

$$RMSE = \sqrt{\frac{1}{N}\sum_{n=1}^{N}\sigma_n^2} \tag{18}$$

To verify our estimation method we have compared the results of our simulations with those of [15] for the rectangular and circular arrays of 8 antenna elements. These comparisons are depicted in Figs. 2and 3 as a function of SNR and the number of snapshots respectively. As it is seen in these figures very good agreement is observed between these results.

Using the same procedure, now we have considered 12 antennas where we can at most distinguish 10 unknowns (5 azimuth angles and 5 elevation angles) as such we can distinguish between 5 simultaneous incident signals (azimuth and elevation) using the MUSIC algorithm.

For this case we presented RMSE of arrival angles versus number of snapshots and the signal to noise ratio (SNR). For comparison of RMSE versus number of snapshots we consider K = 1200 random scenarios for azimuth and elevation angles of arrival with $\hat{\theta}_i \in \left[\frac{-\pi}{2}, \frac{\pi}{2}\right]$ and $\hat{\varphi}_i \in [0, 2\pi]$ for N = 5 simultaneous signals. Simulations were conducted for fixed SNR = 7 dB and variable snapshots between 20 and 200 for different geometries. Fig. 4 shows the RMSE versus number of snapshots for different planar geometries and average amount of RMSE for each configuration is reported in Table 1.

As it is seen in Table 1 for fixed SNR the star planar array has lower average RMSE for estimation angles which is about 21% better than circular planar array.

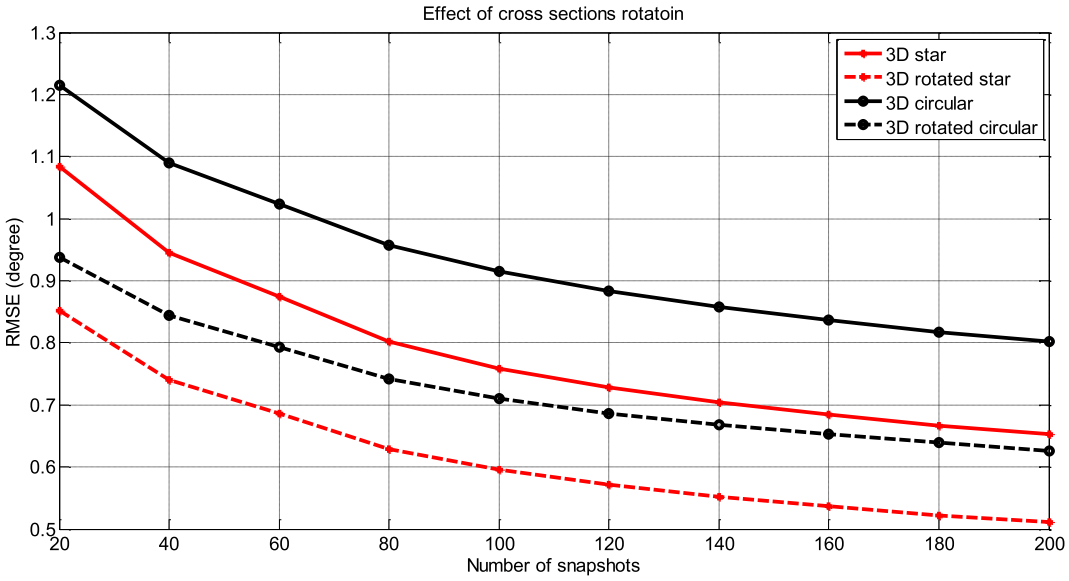

Fig. 12. Comparison of the RMSE of star prism and cylindrical 3D arrays with rotated cross sections to those of normal 3D arrays versus the number of snapshots at fixed SNR = 7 dB.

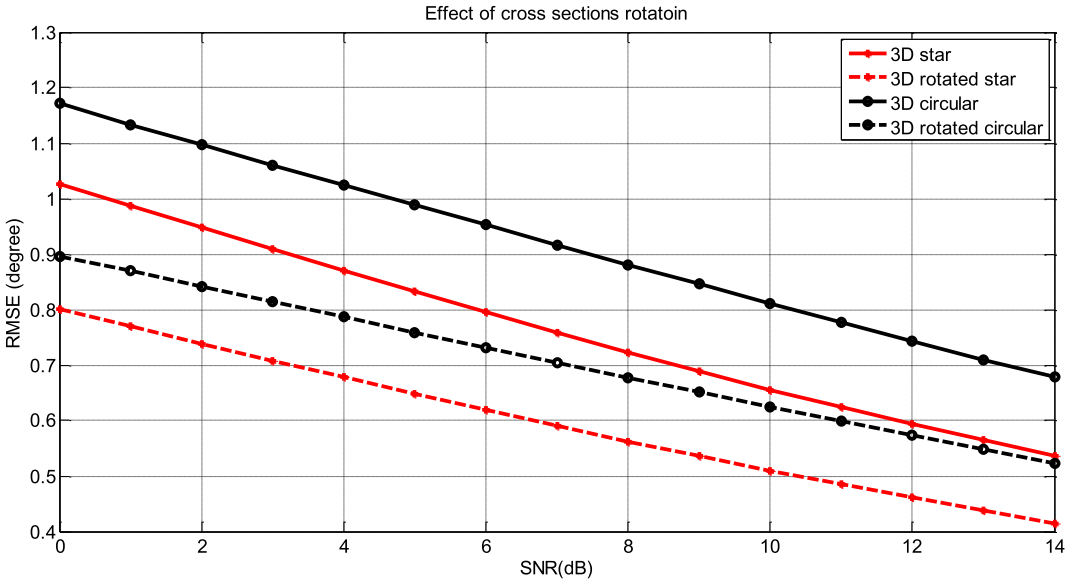

Fig. 13. Comparison of the RMSE of star prism and cylindrical 3D arrays with rotated cross sections to those of normal 3D arrays versus the SNR with fixed number of snapshots L = 100.

After the comparison of RMSE against the number of snapshots for different geometries, simulations were conducted for fixed number of snapshots (i.e. L = 100) and different values of SNR between [0, 14] dB. The number of random scenarios for azimuth and elevation angles is again taken as 1200 and the RMSE versus SNR for different geometries is presented in Fig. 5 and the average of RMSE for each geometry is reported in Table 2.

As it is seen in Table 2 for fixed number of snapshots the star planar array has a better estimation error than the circular planar array of about 22%. In both cases proposed geometries (star and hexagonal) have better resolution than the circular array.

3.2. Three dimensional arrays

In this work the three dimensional configurations consist of three layers of 12 element planar arrays as described before. The antenna layers are distanced by $\lambda/2$ in z direction such that all the arrays have equal volumes. In fact these three dimensional configurations are prisms with cross sections that were introduced in the previous section as planar arrays. Since the cross sectional areas and the heights of prisms are equal, the volume of all configurations are the same. In this case the position vector of antenna elements can be describe by (19).

$$\boldsymbol{r_m} = x_m\hat{x} + y_m\hat{y} + z_m\hat{z} \tag{19}$$

Fig. 6 shows the geometries of different 3D configurations:

In this section the MUSIC DOA estimation algorithm is implemented to compare the RMSE of both azimuth and elevation angles for different 3D geometries with 36 antenna elements and 10 signal sources. Number of random scenarios for arrival angles is considered to be 1200 again and the estimation of error is performed versus the number of snapshots and SNR. Here again the SNR is fixed at 7 dB and the RMSE is calculated for different number of snapshots. The results of these simulations are shown in Fig. 7 and the average of RMSE for different 3D geometries at fixed SNR is reported in Table 3.

As it is seen in Table 3 for 3D configurations the star prism has 24% improvement in comparison to the cylindrical configuration for DOA estimation in the terms of average RMSE.

For 3D geometries in the second case the number of snapshots is fixed at L = 100 and the RMSE is calculated versus SNR as shown in Fig. 8. The average of RMSE for a fixed number of snapshots for each geometries is reported in Table 4.

Again as it is seen in Table 4 the RMSE for star prism array has 16.5% error improvement against cylindrical configuration at fixed number of snapshots. Among different 3D arrays established for DOA estimation in this work the star and the triangular prisms have lowest estimation error.

3.3. Three dimensional arrays with rotated cross sections

A novel geometry is presented in this work as the rotated 3D arrays. For this work we consider 3D prisms used in the previous section and then rotate the top and bottom arrays about the z-axis. In each case the rotation angle about z-axis is $+\varphi_r$ for the top planar array and $-\varphi_r$ for bottom cross section and the middle one is constant. Due to angular periodicity of the arrays the rotation angle of the planar section is $\pi/12$ for the circular, $\pi/6$ for the star and the hexagonal, $\pi/3$ for the triangular and $\pi/4$ for the square arrays. That is, the rotation angle is half the angular period in each case. Fig. 9 shows the new configurations of 3D arrays with rotation angle $\pm\varphi_r$ about the z-axis.

In this case we conducted simulations of Section 3.2 for these novel designs which are named as rotated 3D arrays. The results of DOA estimation error of both azimuth and elevation angles for different arrays are presented in the same manner as before in

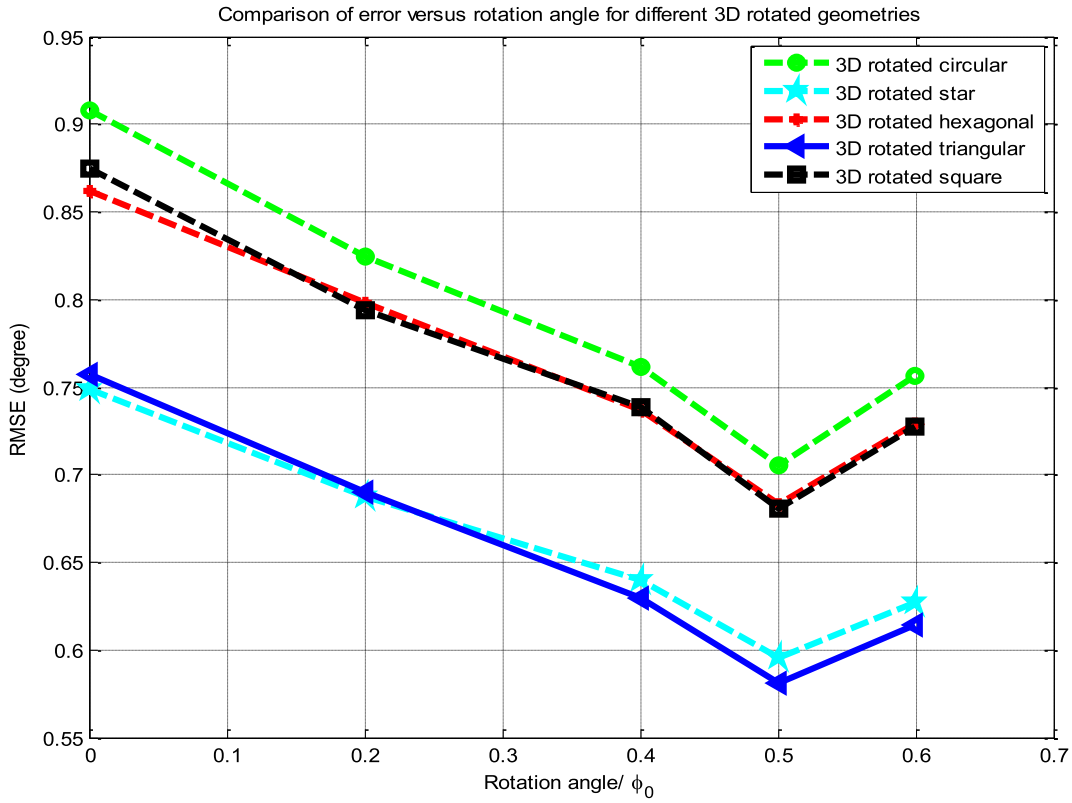

Fig. 14. Comparison of the RMSE for 3D rotated geometries versus the normalized rotation angle with fixed number of snapshots L = 100 and fixed SNR = 7 dB.

Table 7
The values of RMSE (°) for Fig. 14.

Geometry	Angular period (φ_0)	RMSE ($\varphi_r = 0°$)	RMSE ($\varphi_r = 0.2\varphi_0$)	RMSE ($\varphi_r = 0.4\varphi_0$)	RMSE ($\varphi_r = 0.5\varphi_0$)	RMSE ($\varphi_r = 0.6\varphi_0$)
3D Rotated Circular	$\pi/6$	0.908	0.824	0.762	0.705	0.755
3D Rotated Hexagonal	$\pi/3$	0.862	0.798	0.737	0.683	0.729
3D Rotated Square	$\pi/2$	0.874	0.794	0.738	0.681	0.727
3D Rotated Triangular	$2\pi/3$	0.756	0.691	0.630	0.581	0.614
3D Rotated Star	$\pi/2$	0.749	0.688	0.640	0.595	0.632

Figs. 10 and 11. The average of RMSE for simulations versus number of snapshots and SNR are reported in Table 5 and Table 6.

As it is seen in Table 5 at fixed SNR the proposed rotated star and rotated triangular arrays have the lowest RMSE. Table 6 shows that at fixed number of snapshots the rotated star array has 15.5% lower RMSE than rotated circular one.

3.4. Error comparison between the conventional and the rotated cross section 3D arrays

In this case simulations of DOA estimation for 1200 random scenarios of angle of arrivals with 10 sources and 36 antenna elements are compared for rotated cross sections and normal cross sections 3D star and circular configurations. In the first case the SNR is fixed at 7 dB and results are plotted versus number of snapshots, as shown in Fig. 12. The average of RMSE for star prism with rotated cross sections has 41% improvement with respect to normal star prism and the cylindrical 3D array with rotated cross sections has 7% lower average RMSE than normal cylindrical 3D array.

In the second case the results of simulations at fixed number of snapshots are plotted versus SNR for star and circular arrays with rotated cross sections and normal cross sections. Results show that rotated cases have lower estimation error than normal cases, 7.8% for circular and 35% for star 3D arrays, as shown in Fig. 13.

To analyze the RMSE as a function of rotation angle in each geometry of Fig. 9 the SNR is fixed at 7 dB and the number of snapshots is 100 and the number of random scenarios is 1200. Monte-Carlo simulations are conducted for different rotation angles, $\varphi_r = (0, 0.2\varphi_0, 0.4\varphi_0, 0.5\varphi_0, 0.6\varphi_0)^\circ$ for the proposed geometries where φ_0 is the angular period of each array in φ direction. The results of RMSE versus the rotation angles are shown in Fig. 14. In addition the values of RMSE in this case are reported in Table 7 for each geometry of Fig. 9. As it is obvious in Fig. 14 a minimum error point is observed in each case for half a period rotation angle.

4. Conclusion

Different planar array geometries' performances were compared through Monte-Carlo simulations using, MUSIC direction finding algorithm, which showed that the star and the triangular geometries with equal area and a fixed number of elements, have the minimum direction finding estimation error among the 2D geometries which were studied.

Furthermore different 3D array geometries' performances were compared which showed that the star and the triangular prisms with equal volume and equal number of elements have the lowest estimation error in direction finding.

Novel 3D array geometries were introduced. These geometries consisted of rotated cross section 3D geometries. Monte-Carlo simulations showed that the rotated cross section 3D arrays demonstrated a significantly lower estimation error than the normal 3D arrays with the same cross sections. For the triangular cross section rotated 3D geometry, it showed about 24% lower estimation error than the normal prism(with triangular cross section) geometry and for the star cross section rotated 3D geometry it showed about 35% lower estimation error than the normal prism(with star cross section) geometry. Furthermore the star cross section rotated geometry showed about 41% lower estimation error than the normal cylindrical geometry with the same number of elements, as well as the triangular cross section rotated geometry which showed about 42% less error than the standard cylindrical geometry. It is noteworthy that in either of the rotated geometry cases the minimum error was observed for half a period rotation. These novel 3D arrays could give an insight for the implementation of smart antenna arrays intended for new generations of wireless communications.

References

[1] Gross F. Smart Antennas for Wireless Communications. McGraw-Hill Professional; 2005.
[2] Johnson DH. The application of spectral estimation methods. IEEE 1982;70 (9):1018–28.
[3] Capon J. High-resolution frequency-wavenumber spectrum analysis. Proc IEEE 1969;57(8):1408–18.
[4] Schmidt R. Multiple emitter location and signal parameter estimation. IEEE Trans Antennas Propag Mar. 1986;34(3):276–80.
[5] Roy R, Paulraj A, Kailath T. Direction-of-arrival estimation by subspace rotation methods-ESPRIT. Acoust Speech Signal 1986;11:2495–8.
[6] Roy R, Kailath T. ESPRIT-estimation of signal parameters via rotational invariance techniques. IEEE Trans Acoust Jul. 1989;37(7):984–95.
[7] M.M. Abdalla, M.B. Abuitbel, M.A. Hassan, Performance evaluation of direction of arrival estimation using MUSIC and ESPRIT algorithms for mobile communication systems, in: Wireless and Mobile Networking Conference (WMNC), 2013 6th Joint IFIP, 2013, pp. 1–7.
[8] O.A. Oumar, M.F. Siyau, T.P. Sattar, Comparison between MUSIC and ESPRIT direction of arrival estimation algorithms for wireless communication systems, in: The First International Conference on Future Generation Communication Technologies, 2012, pp. 99–103.
[9] Ioannides P, Balanis CA. Uniform circular and rectangular arrays for adaptive beamforming applications. IEEE Antennas Wirel Propag Lett 2005;4(1):351–4.
[10] Ioannides P, Balanis CA. Uniform circular arrays for smart antennas. IEEE Antennas Propag Mag Aug. 2005;47(4):192–206.
[11] Manikas A, Alexiou A, Karimi HR. Comparison of the ultimate direction-finding capabilities of a number of planar array geometries. IEE Proc 1997;144 (6):321–9.
[12] Liang J, Liu D. Two L-shaped array-based 2D DOAs estimation in the presence of MUSIC coupling. Prog Electromag Res January 2011;112:273–98.
[13] M. Hajian, C. Coman, L.P. Ligthart, Comparison of circular, uniform- and non uniform Y-shaped array antenna for DOA estimation using music algorithm, in: Proceedings of the 9th European Conference on Wireless Technology, ECWT 2006, September 2007, vol. 2, pp. 143–146.
[14] R. Sanudin, T. Arslan, Semi-circular antenna array for azimuth DOA estimation, in: Antennas and Propagation Conference (LAPC), 2012 Loughborough, November 2012, pp. 1–4.
[15] Harabi F, Gharsallah A, Marcos S. Three-dimensional antennas array for the estimation of direction of arrival. IET Microwaves Antennas Propag 2009;3 (5):843–9.
[16] Tayem N, Kwon HM. L-shape 2-dimensional arrival angle estimation with propagator method. IEEE Trans Antennas Propag 2005;53(5):1622–30.
[17] Goossens R, Rogier H. Direction-of-arrival and polarization estimation with uniform circular arrays in the presence of mutual coupling. AEU – Int J Electron Commun 2008;62:199–206. http://dx.doi.org/10.1016/j.aeue.2007.03.018.
[18] Gao YF, Zou L, Wan Q. A two-dimensional arrival angles estimation for L-shaped array based on tensor decomposition. AEU – Int J Electron Commun 2015;69:736–44. http://dx.doi.org/10.1016/j.aeue.2015.01.001.
[19] Zhang H, Bi G, Cai Y, Razul SG, See CMS. DOA estimation of closely-spaced and spectrally-overlapped sources using a STFT-based MUSIC algorithm. Digit Signal Process 2016;52:25–34. http://dx.doi.org/10.1016/j.dsp.2016.01.015.